SCIENTIFIC REPORTS

OPEN

Greatly enhanced light emission of MoS$_2$ using photonic crystal heterojunction

Jiang-Tao Liu[1,2,3], Hong Tong[1], Zhen-Hua Wu[4], Jin-Bao Huang[1] & Yun-Song Zhou[5]

We present theoretical study on developing a one-dimensional (1D) photonic crystal heterojunction (h-PhC) that consists of a monolayer molybdenum disulfide (MoS$_2$) structure. By employing the transfer matrix method, we obtained the analytical solution of the light absorption and emission of two-dimensional materials in 1D h-PhC. Simultaneously enhancing the light absorption and emission of the medium in multiple frequency ranges is easy as h-PhC has more modes of photon localization than the common photonic crystal. Our numerical results demonstrate that the proposed 1D h-PhC can simultaneously enhance the light absorption and emission of MoS$_2$ and enhance the photoluminescence spectrum of MoS$_2$ by 2–3 orders of magnitude.

Two-dimensional (2D) transition metal dichalcogenides (TMDCs), such as MoS$_2$ and WSe$_2$, are direct-gap semiconductor 2D materials with excellent optical properties and are thus considered one of the best materials for future optoelectronic devices[1–7]. The light absorption and emission of 2D TMDCs per unit mass are much higher than that of traditional semiconductor materials. 2D TMDCs typically have a thickness of less than 1 nm, and their light absorption and emission are weak, thus limiting their applications in optoelectronic devices. However, due to the benefits of the ultra-thin channel, 2D TMDCs can be combined with optical microstructures, such as photonic crystals, microcavities, and surface plasmas, which effectively enhance the light absorption[8–31] and emission[8,9,32–41] due to the optical localization in these structures. Lien *et al.*[8] and Serkan *et al.*[9] used surface plasmas or optical multilayers to enhance the light absorption and emission of MoS$_2$ or WSe$_2$, thus enhanced the photoluminescence (PL) of MoS$_2$ or WSe$_2$ by 10–30 times.

To further enhance the light emission and absorption of 2D TMDCs, we investigated the effect of photonic crystal heterojunction (h-PhC) on the light absorption and emission of MoS$_2$. Similar to the semiconductor heterojunction, h-PhC comprises photonic crystals (PhC) with different lattice constants or shapes[42]. Earlier studies have found that h-PhC that comprise different PhCs can obtain strong light localization in several frequency ranges[42,43]. On the basis of these findings, one can propose a h-PhC that is formed by different PhCs at intervals to form a multimode high-speed optical waveguide.

Thus, if 2D TMDCs are combined with h-PhC, the strong light localization of h-PhC in multiple frequency ranges can simultaneously enhance the light emission and absorption of 2D TMDCs. We therefore conducted a detailed study on a h-PhC which consists of 1D PhCs with two kinds of crystal lattices that form an h-PhC microcavity structure. To thoroughly understand the light absorption and emission in h-PhC, we first identified the analytical solution of the light absorption and emission of MoS$_2$ in h-PhC. The findings indicate that h-PhC can enhance the light absorption and emission of MoS$_2$ and enhance the PL spectrum of MoS$_2$ by 2–3 orders of magnitude, which has a promising prospect and important application value in fluorescent probe, 2D LED, etc. The analytical solution can be used not only for the light absorption and emission in h-PhC but also for the calculation of other 1D PhC-2D materials composite structures.

Model and Theory

The structure of h-PhC is shown in Fig. 1, i.e., $(A_1B_1)^{N_1}C_1MC_2(B_2A_2)^{N_2}$ structure. $(A_1B_1)^{N_1}$ and $(B_2A_2)^{N_2}$ layers constitute the two distributed Bragg reflectors (DBRs), where N_1 and N_2 are the numbers of cycles. The A_1 and A_2

[1]College of Mechanical and electrical engineering, Guizhou Minzu University, Guiyang, 550025, China. [2]Department of Physics, Nanchang University, Nanchang, 330031, China. [3]Institute for Advancfed Study, Nanchang University, Nanchang, 330031, China. [4]Key Laboratory of Microelectronic Devices and Integrated Technology, Institute of Microelec-tronics, Chinese Academy of Sciences, Beijing, 100029, China. [5]Department of Physics, Capital Normal University, Beijing, 100037, China. Correspondence and requests for materials should be addressed to J.-T.L. (email: jtliu@semi.ac.cn) or Y.-S.Z. (email: 263zys@263.net)
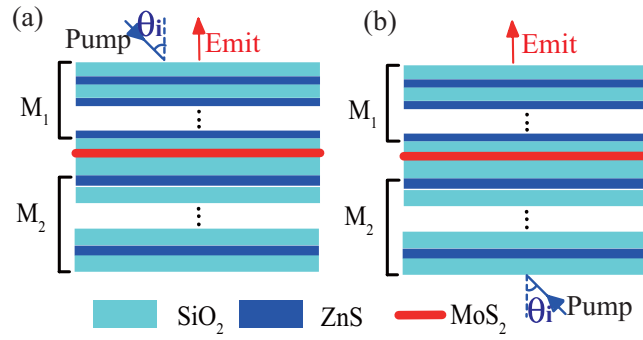
1

Figure 1. Schematic of h-PhC structure. (**a**) Pump light and outgoing light on the same side; (**b**) pump light and outgoing light on different sides.

layers are made of SiO$_2$ with the permittivity $n_{SiO_2} = 1.4923 + 0.81996\lambda'^2/(\lambda'^2 - 0.10396^2) - 0.01082\lambda'^2$[44]. $\lambda' = \lambda \times 10^6$, λ is wavelength of the input light beams, and the thicknesses of the A_1 and A_2 layers are $\lambda_{10}/(4 \times 1.53)$ and $\lambda_{20}/(4 \times 1.53)$, respectively. λ_{10} and λ_{20} are the center wavelengths of the the upside PhC and the bottom PhC, respectively. B_1 and B_2 layers are composed of ZnS with the permittivity $n_{ZnS} = 8.393 + 0.14383/(\lambda'^2 - 0.2421^2) + 4430.99/(\lambda'^2 - 36.72^2)$[45]. The thicknesses of the B_1 and B_2 layers are $\lambda_{10}/(4 \times 2.4)$ and $\lambda_{20}/(4 \times 2.4)$. The C_1 and C_2 layers are made of SiO$_2$, and their thicknesses are d_{C_1} and d_{C_2}, respectively. The M layer is the MoS$_2$ layer. Its thickness is 0.65 nm.

To model the absorption of MoS$_2$ in this structure, the transfer matrix method is used first[46,22]. In the l-th layer, the electric field of the TE mode light beam with incident angle θ_t is given by

$$\mathbf{E}_l(x, y) = [A_l e^{ik_x(x-x_l)} + B_l e^{-ik_x(x-x_l)}]e^{ik_y y}\mathbf{e}_z, \tag{1}$$

where $k_l = k_{lr} + ik_{li}$ is the wave vector of the incident light, $\mathbf{e}_z$ is the unit vectors in the z direction, and x_i is the position of the l-th layer in the x direction. And the magnetic field of the TM mode in the l-th layer is given by

$$\mathbf{H}_l(x, y) = [A_l e^{ik_x(x-x_l)} + B_l e^{ik_x(x-x_l)}]e^{ik_y y}\mathbf{e}_z, \tag{2}$$

The electric (magnetic) fields of TE (TM) mode in the $(l+1)$-th and l-th layer are related by the matrix utilizing the boundary condition

$$\begin{pmatrix} A_{l+1} \\ B_{l+1} \end{pmatrix} = \begin{pmatrix} \dfrac{\gamma_l + \gamma_{l+1}}{2\gamma_{l+1}}e^{ik_x d_l} & \dfrac{\gamma_{l+1} - \gamma_l}{2\gamma_{l+1}}e^{-ik_x d_l} \\ \dfrac{\gamma_{l+1} - \gamma_l}{2\gamma_{l+1}}e^{ik_x d_l} & \dfrac{\gamma_l + \gamma_{l+1}}{2\gamma_{l+1}}e^{-ik_x d_l} \end{pmatrix} \begin{pmatrix} A_l \\ B_l \end{pmatrix} = T^{l+1 \leftarrow l}\begin{pmatrix} A_l \\ B_l \end{pmatrix}, \tag{3}$$

where $\gamma_l = \dfrac{k_{lx}^r + ik_{lx}^i}{\mu_l(\omega)}$ $\left(\gamma_l = \dfrac{k_{lx}^r + ik_{lx}^i}{\varepsilon_l(\omega)}\right)$ for TE (TM) mode, $\mu_l(\omega)$ is the permeability, $\varepsilon_l(\omega) = \varepsilon_l^r(\omega) + i\varepsilon_l^i(\omega)$ is the complex dielectric permittivity, and d_1 is the thickness of the l-th layer. Thus, the fields in the $(l+1)$-th layer are related to the incident fields by the transfer matrix

$$\begin{pmatrix} A_{l+1} \\ B_{l+1} \end{pmatrix} = T^{l+1 \leftarrow l} \cdots T^{2 \leftarrow 1} T^{1 \leftarrow 0}\begin{pmatrix} A_0 \\ B_0 \end{pmatrix} = \begin{pmatrix} T_{11} & T_{12} \\ T_{21} & T_{22} \end{pmatrix}\begin{pmatrix} A_0 \\ B_0 \end{pmatrix}. \tag{4}$$

To thoroughly describe the light absorption and emission of MoS$_2$ in h-PhC, improve the computational speed to optimize the structure, and help scholars who are not familiar with the transfer matrix method for computing, we obtained the analytical solutions of the light absorption and emission of MoS$_2$ in h-PhC using the transfer matrix method. Since the transfer matrix of the electric fields of TE mode and the transfer matrix of magnetic fields of TM mode have the same form, we only show the analytical solution of the TE mode. First, for a N-period PhC in air, the transfer matrix can be written as[47].

$$\begin{pmatrix} A_0 \\ B_0 \end{pmatrix} = M_N \begin{pmatrix} A_{l+1} \\ B_{l+1} \end{pmatrix} = \begin{bmatrix} 1/t_N & r_N^*/t_N^* \\ r_N/t_N & 1/t_N^* \end{bmatrix}\begin{pmatrix} A_{l+1} \\ B_{l+1} \end{pmatrix}, \tag{5}$$

where $\dfrac{1}{t_N} = \dfrac{1}{t_0}\dfrac{\sin N\beta}{\sin\beta} - \dfrac{\sin(N-1)\beta}{\sin\beta}, \dfrac{r_N}{t_N} = \dfrac{r_0}{t_0}\dfrac{\sin N\beta}{\sin\beta}$, β is the Bloch phase in each period, t_0 and r_0 are the transmission amplitude and reflection amplitude of the each period[47]. For the upper part PhC in the h-PhC, the right hand side is not air. By multiplying the transfer matrix of PhC to the C_1 layer $T^{C \leftarrow P}(d_c = 0)$ and the inverse transfer matrix of PhC to the air layer $[T^{air \leftarrow P}(d_c = 0)]^{-1}$, we can get the transfer matrix of the upper part PhC

$$\left(M'_{N_1}\right) = \left\{ M_{N_1} T^{C\leftarrow P}(d_c = 0)[T^{air\leftarrow P}(d_c = 0)]^{-1} \right\}^{-1}$$

$$= \frac{1}{2}\begin{pmatrix} \zeta/t_{N_1} + \zeta'r^*_{N_1}/t^*_{N_1} & \zeta't_{N_1} + \zeta r^*_{N_1}/t^*_{N_1} \\ \zeta r_{N_1}/t_{N_1} + \zeta'/t^*_{N_1} & \zeta'r_{N_1}/t_{N_1} + \zeta/t^*_{N_1} \end{pmatrix}$$

$$= \begin{bmatrix} 1/t'_{N_1} & r'^*_{N_1}/t'^*_{N_1} \\ r'_{N_1}/t'_{N_1} & 1/t'^*_{N_1} \end{bmatrix}, \tag{6}$$

where $\zeta = 1 + \sqrt{\varepsilon_c}\cos\theta_c$, $\zeta' = 1 - \sqrt{\varepsilon_c}\cos\theta_c$, $\varepsilon_c = \varepsilon_{c_1} = \varepsilon_{c_2}$ is the permittivity of C_1 and C_2 layers, $\theta_c = \theta_{c_1} = \theta_{c_2}$ is the propagation angle in the C_1 and C_2 layer. Similar, we can get the transfer matrix of the lower part PhC,

$$M'_{N_2} = \left\{ [T^{C\leftarrow P}(d_c = 0)]^{-1} T^{air\leftarrow E}(d_c = 0) \right\} M_{N_2}$$

$$= \frac{1}{2}\begin{pmatrix} \zeta/t_{N_2} + \zeta'r_{N_2}/t_{N_2} & \zeta'/t^*_{N_2} + \zeta r^*_{N_2}/t^*_{N_2} \\ \zeta r_{N_2}/t_{N_2} + \zeta'/t_{N_2} & \zeta'r^*_{N_2}/t^*_{N_2} + \zeta/t^*_{N_2} \end{pmatrix}$$

$$= \begin{bmatrix} 1/t'_{N_2} & r'^*_{N_2}/t'^*_{N_2} \\ r'_{N_2}/t'_{N_2} & 1/t'^*_{N_2} \end{bmatrix}. \tag{7}$$

The transfer matrix of the C_1 layer is[11].

$$M_f(d_{C_1}) = \begin{bmatrix} e^{-ik_{cx}d_{C_1}} & 0 \\ 0 & e^{ik_{cx}d_{C_1}} \end{bmatrix}, \tag{8}$$

and the transfer matrix of the C_2 layer is

$$M_f(L_{cav} - d_{C_1}) = \begin{bmatrix} e^{-ik_{cx}(L_{cav}-d_{C_1})} & 0 \\ 0 & e^{ik_{cx}(L_{cav}-d_{C_1})} \end{bmatrix}, \tag{9}$$

where $L_{cav} = d_{C_1} + d_{C_2}$ is the microcavity length, k_{cx} is the wave vector of the light in the C_1 or C_2 layer. Taking the approximation that $e^{ik_{Mx}d_M} \approx 1 + ik_{Mx}d_M$, where k_{Mx} is the wave vector of the light in the MoS$_2$ layer and d_M is the thickness of the and MoS$_2$ layer, the transfer matrix of the MoS$_2$ layer is

$$M_{MoS_2} = [T^{C\leftarrow MoS_2}T^{MoS_2\leftarrow C}(d=0)]^{-1} = \begin{bmatrix} 1 - \eta_1 & -\eta_2 \\ \eta_2 & 1 + \eta_1 \end{bmatrix}, \tag{10}$$

where $\eta_1 = ik_{Mx}d_M\left[\left(\sqrt{\varepsilon_{MoS_2}/\varepsilon_c}\cos\theta_{MoS_2}/\cos\theta_c\right) + \left(\sqrt{\varepsilon_c/\varepsilon_{MoS_2}}\cos\theta_c/\cos\theta_{MoS_2}\right)\right]/2$, and $\eta_2 = ik_{Mx}d_M\left[\left(\sqrt{\varepsilon_{MoS_2}/\varepsilon_c}\cos\theta_{MoS_2}/\cos\theta_c\right) - \left(\sqrt{\varepsilon_c/\varepsilon_{MoS_2}}\cos\theta_c/\cos\theta_{MoS_2}\right)\right]/2$. Thus, the total transfer matrix of the C_1, C_2, and MoS$_2$ layer is

$$M_f(d_{C_1})M_{MoS_2}M_f(L - d_{C_1}) = \begin{bmatrix} (1 - \eta_1)e^{-ikL} & -\eta_2 e^{ik(L-2d_{C_1})} \\ \eta_2 e^{-ik(L-d_{C_1})} & (1 + \eta_1)e^{ikL} \end{bmatrix}. \tag{11}$$

The total transfer matrix of the h-PhC is

$$M = M'_{N_1}M_f(d_{C_1})M_{MoS_2}M_f(L - d_{C_1})M'_{N_2}. \tag{12}$$

We can get the matrix element

$$M_{11} = \left[(1 - \eta_1)/\varphi_1 t'_{N_1} - \eta_2\varphi_2 r'_{N_2}/t'_{N_1} + \eta_2 r'^*_{N_1}/\varphi_2 t'^*_{N_1} + (1 + \eta_1)\varphi_1 r'_{N_2}r'^*_{N_1}/t'^*_{N_1}\right]/t'_{N_2}, \tag{13}$$

and

$$M_{21} = \left[(1 - \eta_1)r'_{N_1}/\varphi_1 t'_{N_1} - \eta_2\varphi_2 r'_{N_2}r'_{N_1}/t'_{N_1} + \eta_2/\varphi_2 t'^*_{N_1} + (1 + \eta_1)\varphi_1 r'_{N_2}/t'^*_{N_1}\right]/t'_{N_2}, \tag{14}$$

where $\varphi_1 = e^{ikL}$, $\varphi_2 = e^{ik(L-2d_{C_1})}$. The transmittance of the h-PhC is $T = |1/M_{11}|^2$; the reflectance of the h-PhC is $R = |M_{21}/M_{11}|^2$[11,47] the absorption of MoS$_2$ layer is $A_{MoS_2} = 1 - R - T$.

The spontaneous emission of the monolayer MoS$_2$ in the h-PhC can be treated as two emitted correlated wave-packets, upward (downward) propagating wave packet $\mathcal{P}_u$ ($\mathcal{P}_d$). The emission wavepackets are partially transmitted and reflected by the two DBRs. The filed amplitude of the light emitted out from the exit DBR mirror is given by[48–50].
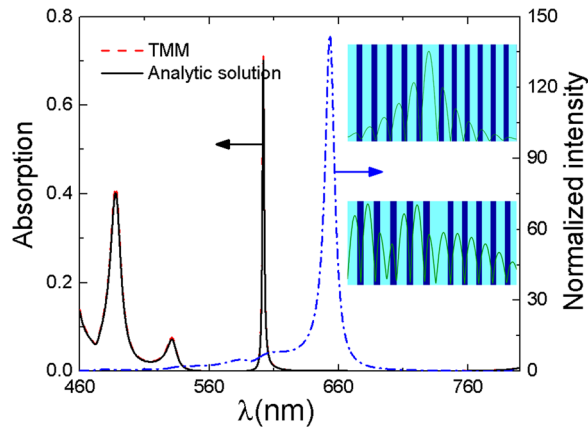
Figure 2. The absorption and relative radiation intensity of MoS$_2$ when the pump and outgoing lights are on the same side of the h-PhC. The black solid line and the red dashed line are the calculation results of the analytical solution and the transfer matrix method, respectively. The upper and lower illustrations are the light field distribution at wavelengths of 488 and 602 nm, respectively.

$$
\begin{aligned}
E_{DBRt}(t) \;=\; & t_t \mathcal{P}(t) + t_t r_b \mathcal{P}\!\left(t - \frac{2z_{ol}}{c}\right) \\
& + t_t(r_b r_t)\mathcal{P}\!\left(t - \frac{2L_{oc}}{c}\right) \\
& + t_t(r_b r_b r_t)\mathcal{P}\!\left(t - \frac{2z_{ol}}{c} - \frac{2L_{oc}}{c}\right) + \cdots,
\end{aligned}
\tag{15}
$$

where r_t and t_t are the reflection amplitude and transmission amplitude of the exit DBR mirror, respectively. r_b is the reflection amplitude of the back DBR mirror, z_{ol} is the distance between the monolayer MoS$_2$ and back DBR mirror. When the pumping and outgoing lights are on the same side of the h-PhC, $r_t = r'_{N_1}$, $t_t = t'_{N_1}$, $r_b = r'_{N_2}$, $z_{ol} = d_{C_2}$; When the pumping and outgoing lights are on the opposite side of the h-PhC, $r_t = r'_{N_2}$, $t_t = t'_{N_2}$, $r_b = r'^2_{N_1}$, $z_{ol} = d_{C_1}$; $\mathcal{P}(t)$ is the electric amplitude against time for a single emission event (in either direction), $L_{oc} = n_c L_{cav} = n_c(d_{C_1} + d_{C_2})$ is the optical length of microcavity, n_c is the permittivity of the C$_1$ and C$_2$ layer. By using the Fourier transform, the emitted radiation from the top DBR mirror in the frequency domain can be written as

$$
\begin{aligned}
E_{DBRt}(\omega) \;=\; & \frac{t_t}{2\pi} \int_{-\infty}^{\infty} \mathcal{P}(t)\exp(i\omega t)dt \\
& + \frac{t_t r_b}{2\pi} \int_{-\infty}^{\infty} \mathcal{P}\!\left(t - \frac{2z_{ol}}{c}\right)\exp(i\omega t)dt \\
& + \frac{t_t(r_b r_t)}{2\pi} \int_{-\infty}^{\infty} \mathcal{P}(t - \frac{2L_{oc}}{c})\exp(i\omega t)dt \\
& + \frac{t_t(r_b r_b r_t)}{2\pi} \int_{-\infty}^{\infty} \mathcal{P}\!\left(t - \frac{2z_{ol}}{c} - \frac{2L_{oc}}{c}\right) \\
& \times \exp(i\omega t)dt + \cdots.
\end{aligned}
\tag{16}
$$

Neglecting the changes of the spontaneous time, integral of Eq. (16), the emission intensity can be calculated by[48,49].

$$
|E_{DBRt}(\lambda)|^2 = \frac{1 + R_b + 2\sqrt{R_b}\,\cos\!\left(\frac{4\pi n_c Z_{OL}}{\lambda}\right)}{1 + R_b R_t - 2\sqrt{R_b R_t}\,\cos\!\left(\frac{4\pi n_c L_{cav}}{\lambda}\right)} \times T_t |\mathcal{P}(\lambda)|^2,
\tag{17}
$$

where $T_t = |t_t|^2$ and $R_t = |r_t|^2$ are the transmittance and reflectance of the exit DBR mirror, respectively, $T_b = |t_b|^2$ and $R_b = |r_b|^2$ are the the transmittance and reflectance of the back DBR mirror with the MoS$_2$ TFT, respectively.

Results

We first calculated the absorption and the relative radiation intensity of MoS$_2$ when the pumping and outgoing lights are on the same side of the h-PhC. The optimized parameters are as follows: $\lambda_{10} = 730\,\text{nm}$, $\lambda_{20} = 630\,\text{nm}$, $d_{C_1} = 0\,\text{nm}$, $d_{C_2} = 214\,\text{nm}$, $N_1 = 6$, and $N_2 = 7$. The incident angle is $\theta_i = 48°$. The pumping light is in TE mode. The outgoing light is vertically emitted. The calculation results are shown in Fig. 2. Two strong absorption peaks
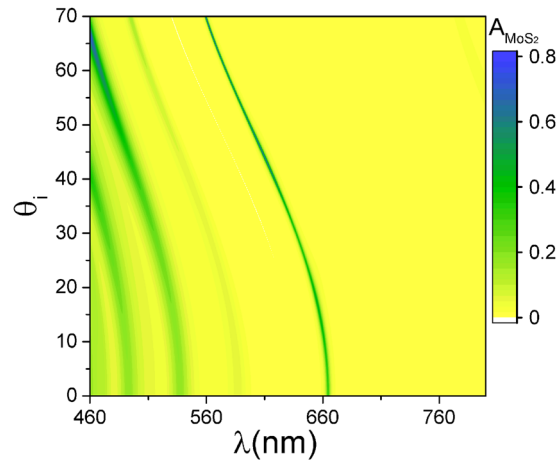
Figure 3. h-PhC MoS$_2$ absorption changes as the incident angle and wavelength change.

emerge at wavelengths of 488 nm (consistent with the wavelength of the pump light used in the experiment[9]) and 602 nm. Quite small difference can be found between the numerical transfer matrix method and the calculation results from the analytical solution with the approximation $e^{ik_{Mx}d_M} \approx 1 + ik_{Mx}d_M$. The optical wavelength of 602 nm is in the bandgap of the two PhCs with strong localization properties (upper illustration of Fig. 1) and strong absorption. The absorption can reach 0.7 or more, which is approximately 6 times larger than that without h-PhC. If the wavelength of the pumping light is 488 nm, it is only in the bandgap of the bottom PhC. The localization is weak. The absorption is 0.4, which is about 3 times larger than that without h-PhC. The emission efficiency is enhanced by 140 times due to the high reflectivity of the PhCs on both sides. Thus, when the lights are of 488 nm and 602 nm wavelengths, the PL is enhanced by approximately 420 and 840 times, respectively.

The MoS$_2$ absorption in h-PhC is sensitive to the incidence angle. The calculation results are shown in Fig. 3. The resonant wavelength of the microcavity satisfies the relation ship $m_0\lambda_c/2 = L_c \cos\theta'$. $L_c = n_c d_c$ is the microcavity optical path, m_0 is a positive integer, and $\theta' = arcsin\theta_i/n_c$ is the propagation angle of light in the defective layer. Thus, when the incident angle increases, the resonance wavelength moves in the short-wave direction, the reflectivities of the PhCs on both sides increases, the travel path of light in MoS$_2$ increases, and the maximum absorption can reach 0.8 or more. PL is enhanced by approximately 3 orders of magnitude.

We also calculated the positive incidence of the pumping light and the absorption and relative radiation intensity of MoS$_2$ when the pumping and outgoing lights are on opposite sides of the h-PhC. According to the experiment[9], in our calculation, the wavelength of the pumping light is 488 nm, and the wavelength of the outgoing light approaches 660 nm. We calculated the corresponding parameters by optimizing the h-PhC structure under different pumping light incidences as follows: when the pumping light is normally incident and the pumping and outgoing lights are on the same side of the h-PhC, $\lambda_{10} = 580$ nm, $\lambda_{20} = 610$ nm, $d_{C_1} = 2$ nm, $d_{C_2} = 214$ nm, $N_1 = 7$, and $N_2 = 7$. When the pumping light is normally incident and the pumping and outgoing lights are on opposite sides of the h-PhC, $\lambda_{10} = 630$ nm, λ_{20} 570 nm, $d_{C_1} = 11$ nm, $d_{C_2} = 203$ nm, $N_1 = 7$, and $N_2 = 7$. When the pumping light is obliquely incident and the pumping and outgoing lights are on opposite sides of the h-PhC, $\lambda_{10} = 660$ nm, $\lambda_{20} = 580$ nm, $d_{C_1} = 0$ nm, $d_{C_2} = 216$ nm, $N_1 = 7$, $N_2 = 7$, and $\theta_i = 30°$.

The detailed calculation results are shown in Fig. 4. Regardless of whether the pumping and outgoing lights are on the same or different sides of the h-PhC, the absorption of MoS$_2$ is higher when the pumping light is obliquely incident. A strong local touch in the vicinity of two wavelengths can be easily obtained as change in incidence angle can adjust the resonant wavelength. When the pumping light is normally incident and the pumping and outgoing lights are on opposite sides of the h-PhC, the absorption of MoS$_2$ is high because if MoS$_2$ in the microcavity structure obtains strong absorption and emission, the reflectivity of the rear reflector should be higher but the reflectivity of the front reflector should not be excessively high[19]. The bandgap width of the PhC is not big enough due to the large difference between the wavelengths of the pumping and outgoing lights. The pumping and outgoing lights on different sides realize this goal easily.

For comparison, we calculated the light absorption and emission of MoS$_2$ in a homojunction. The optimized structural parameters are as follows: when the pumping light is obliquely incident and the pumping and outgoing lights are on the same side, $\lambda_{10} = \lambda_{20} = 660$ nm, $d_{C_1} = 0$ nm, $d_{C_2} = 215$ nm, $N_1 = 5$, $N_2 = 7$, and $\theta_i = 42°$. When the pumping light is normally incident and the pumping and outgoing lights are on the same side, $\lambda_{10} = \lambda_{20} = 680$ nm, $d_{C_1} = 4$ nm, $d_{C_2} = 210$ nm, $N_1 = 5$, and $N_2 = 7$. When the pumping light is obliquely incident and the pumping and outgoing lights are on opposite sides, $\lambda_{10} = \lambda_{20} = 670$ nm, $d_{C_1} = 0$ nm, $d_{C_2} = 214$ nm, $N_1 = 6$, $N_2 = 5$, and $\theta_i = 54°$. When the pumping light is normally incident and the pumping and outgoing lights are on opposite sides: $\lambda_{10} = \lambda_{20} = 650$ nm, $d_{C_1} = 0$ nm, $d_{C_2} = 214$ nm, $N_1 = 6$, and $N_2 = 5$. The calculation results are shown in Fig. 5. These structures show that the localization of homojunction PhC is not excessive and increasing the light absorption and emission of MoS$_2$ at the same time is difficult. When the light emission is strong, the light absorption is usually low, with an absorption of only approximately 0.2. When the pumping light
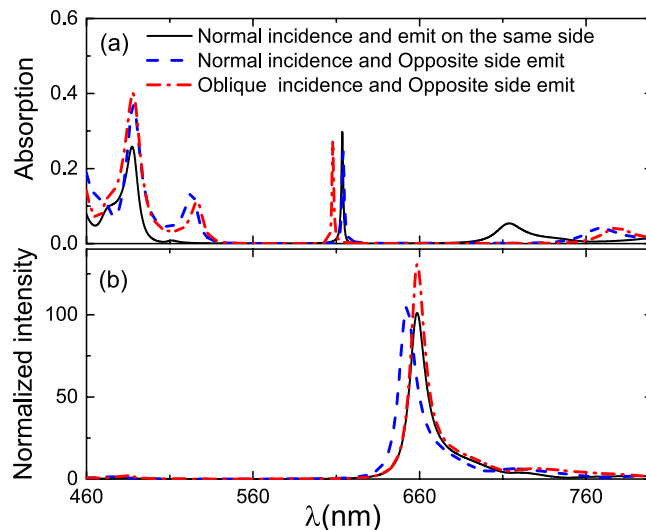
Figure 4. (**a**) Light absorption and (**b**) light emission of MoS_2 in h-PhC under different pump lights. The black solid line: when the pump light is normally incident, the pump and outgoing lights are in the same side of the h-PhC; the blue dashed line: when the pump light is normally incident, the pump and outgoing lights are on opposite sides of the h-PhC; the r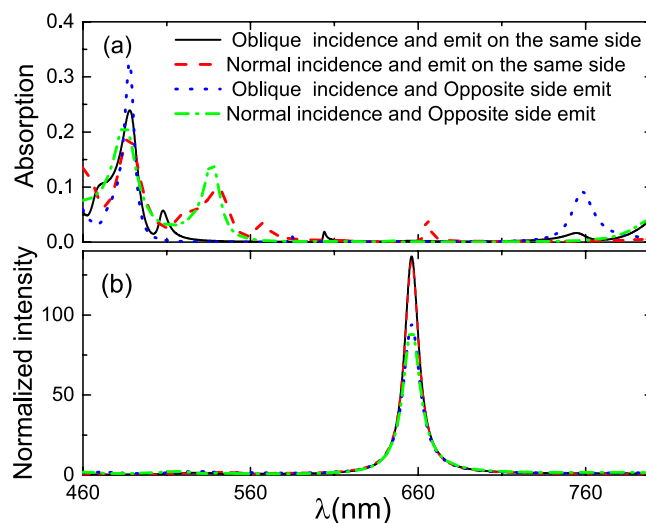ed dash-dotted line: when the pump light is obliquely incident, the pump and outgoing lights are on opposite sides of the h-PhC.

Figure 5. (**a**) Light absorption and (**b**) light emission of MoS_2 in homojunction PhC under different pumping lights. The black solid line: when the pumping light is obliquely incident and the pumping and outgoing lights are on the same side; the red dashed line: when the pumping light is normally incident and the pumping and outgoing lights are on the same side; the blue dotted line: when the pumping light is obliquely incident and the pumping and outgoing lights are on opposite sides; the green dash-dotted line: when the pumping light is normally incident and the pumping and outgoing lights are on opposite sides.

is obliquely incident and the pumping and outgoing lights are on opposite sides, the absorption is the largest (approximately 0.33) but the outgoing light enhancement is low. If light emission is enhanced using longer PhC cycles than those used in the current study, the light absorption of MoS_2 will decrease. However, this case does not happen in h-PhC.

Finally, we discuss the effect of light localization and the feasibility of the experiment.

The effect of light localization: We used the Q value to judge the strength of light localization. The larger the Q value, the higher the light localization and light absorption and emission intensity of MoS_2. However, the higher the Q value, the smaller the full width at half maximum of the spectral line and the narrower the absorption and PL spectra. Excessively narrow absorption and emission spectra are not conducive to practical application. Moreover, when the Q value is high, the microcavity affects the transition time of the exciton. Thus, in Optimizing the parameters, we choose $N_1 \leq 7$ and $N_2 \leq 7$.

The feasibility of the experiment: PhC and 2D materials composite structures (particularly 2D materials-PhC microcavity) were created [14–16]. Compared with the existing structure, this structure only changes the lattice constant of the upper and lower reflectors of the PhC microcavity. Therefore, the experiment is completely achievable.

Conclusion

We studied the effect of 1D h-PhC on the light absorption and emission of monolayer MoS_2 and obtained the solutions of both light absorption and emission in 1D PhC-2D materials composite structures. h-PhC has more models of photon localization than common PhC, which enhances the light emission and absorption of MoS_2 simultaneously, and increases the PL spectrum of MoS_2 by 2–3 orders of magnitude. When the pumping light is obliquely incident and the pumping and outgoing lights are on opposite sides of the h-PhC, it is easier to enhance the light absorption and emission of MoS_2 at the same time. The analytical solution can be used not only for light absorption and emission in h-PhC but also applicable for other 1D PhC-2D materials composite structures. This study has a promising prospect and important application value in 2D material-based optoelectronic devices.

Methods

The modified transfer matrix method is used to model the absorption of monolayer MoS_2 in the photonic crystal micro-cavity.

References

1. Wang, Q. H., Kalantar-Zadeh, K., Kis, A., Coleman, J. N. & Strano, M. S. Electronics and optoelectronics of two-dimensional transition metal dichalcogenides. *Nat. Nanotech.* **7**, 699–712 (2012).
2. Congxin, X. & Jingbo, L. Recent advances in optoelectronic properties and applications of two-dimensional metal chalcogenides. *Journal of Semiconductors* **37**, 051001, http://stacks.iop.org/1674-4926/37/i=5/a=051001 (2016).
3. Mak, K. F., Lee, C., Hone, J., Shan, J. & Heinz, T. F. Atomically thin MoS_2: a new direct-gap semiconductor. *Phys. Rev. Lett.* **105**, 136805 (2010).
4. Splendiani, A. *et al.* Emerging photoluminescence in monolayer MoS_2. *Nano Lett.* **10**, 1271–1275 (2010).
5. Lopez-Sanchez, O., Lembke, D., Kayci, M., Radenovic, A. & Kis, A. Ultrasensitive photodetectors based on monolayer MoS_2. *Nat. Nanotech.* **8**, 497–501 (2013).
6. Guo, C. F., Sun, T., Cao, F., Liu, Q. & Ren, Z. Metallic nanostructures for light trapping in energy-harvesting devices. *Light: Science & Applications* **3**, e161 (2014).
7. Wang, F. *et al.* Progress on electronic and optoelectronic devices of 2d layered semiconducting materials. *Small* 1604298 (2017).
8. Lien, D.-H. *et al.* Engineering light outcoupling in 2d materials. *Nano Lett.* **15**, 1356–1361 (2015).
9. Butun, S., Tongay, S. & Aydin, K. Enhanced light emission from large-area monolayer mos2 using plasmonic nanodisc arrays. *Nano Lett.* **15**, 2700–2704 (2015).
10. Thongrattanasiri, S., Koppens, F. H. L. & de Abajo, F. J. G. Complete optical absorption in periodically patterned graphene. *Phys. Rev. Lett.* **108**, 047401 (2012).
11. Ferreira, A., Peres, N. M. R., Ribeiro, R. M. & Stauber, T. Graphene-based photodetector with two cavities. *Phys. Rev. B* **85**, 115438 (2012).
12. Ferreira, A. & Peres, N. M. R. Complete light absorption in graphene-metamaterial corrugated structures. *Phys. Rev. B* **86**, 205401 (2012).
13. Wang, W. *et al.* Enhanced absorption in two-dimensional materials via fano-resonant photonic crystals. *Appl. Phys. Lett.* **106**, 181104 (2015).
14. Furchi, M. *et al.* Microcavity-integrated graphene photodetector. *Nano Lett.* **12**, 2773–2777 (2012).
15. Engel, M. *et al.* Lightcmatter interaction in a microcavity-controlled graphene transistor. *Nature Communications* **3**, 906 (2012).
16. Liu, X. *et al.* Strong lightcmatter coupling in two-dimensional atomic crystals. *Nature Photonics* **9**, 30–34 (2015).
17. Sandhu, S., Yu, Z. & Fan, S. Detailed balance analysis and enhancement of open-circuit voltage in single-nanowire solar cells. *Nano Lett.* **14**, 1011–1015 (2014).
18. Zhang, Z. Z., Chang, K. & Peeters, F. M. Tuning of energy levels and optical properties of graphene quantum dots. *Phys. Rev. B* **77**, 235411 (2008).
19. Vincenti, M. A., de Ceglia, D., Grande, M., D'Orazio, A. & Scalora, M. Nonlinear control of absorption in one-dimensional photonic crystal with graphene-based defect. *Opt. Lett.* **38**, 3550–3553 (2013).
20. Guozhi, J., Peng, W., Yanbang, Z. & Kai, C. Localized surface plasmon enhanced photothermal conversion in bi2se3 topological insulator nanoflowers. *Sci Rep.* **6**, 25884 (2016).
21. Shuyuan, X. *et al.* Tunable light trapping and absorption enhancement with graphene ring arrays. *Phys. Chem. Chem. Phys.* **18**, 26661–26669 (2016).
22. Wu, Y.-B., Yang, W., Wang, T.-B., Deng, X.-H. & Liu, J.-T. Broadband perfect light trapping in the thinnest monolayer graphene-mos2 photovoltaic cell: the new application of spectrum-splitting structure. *Scientific Reports* **6**, 20955 (2016).
23. Zheng, J., Barton, R. A. & Englund, D. Broadband coherent absorption in chirped-planar-dielectric cavities for 2d-material-based photovoltaics and photodetectors. *ACS Photonics* **1**, 768–774 (2014).
24. Linshuang, L., Yue, Y., Hong, Y. & Liping, W. Optical absorption enhancement in monolayer mos2 using multi-order magnetic polaritons. *Journal of Quantitative Spectroscopy and Radiative Transfer* **200**, 198–205 (2017).
25. Zhao, C. X., Xu, W., Li, L. L., Zhang, C. & Peeters, F. M. Terahertz plasmon-polariton modes in graphene driven by electric field inside a fabry-prot cavity. *Journal of Applied Physics* **117**, 223104 (2015).
26. Zu, S. *et al.* Active control of plasmon-exciton coupling in mos2-ag hybrid nanostructures. *Advanced Optical Materials* **4**, 1463–1469 (2016).
27. Wang, M. *et al.* Plasmon-trion and plasmon-exciton resonance energy transfer from a single plasmonic nanoparticle to monolayer mos2. *Nanoscale* C7NR03909C, https://doi.org/10.1039/C7NR03909C (2017).
28. Jeong, H. Y. *et al.* Optical gain in mos2 via coupling with nanostructured substrate: Fabry-perot interference and plasmonic excitation. *ACS Nano* **10**, 8192–8198 (2016).
29. Lu, H. *et al.* Nearly perfect absorption of light in monolayer molybdenum disulfide supported by multilayer structures. *Opt. Express* **25**, 21630–21636 (2017).
30. Yao, Z. *et al.* Tunable surface-plasmon-polariton-like modes based on graphene metamaterials in terahertz region. *Computational Materials Science* **117**, 544–548 (2016).
31. Ansari, N. & Mohebbi, E. Increasing optical absorption in one-dimensional photonic crystals including mos2 monolayer for photovoltaics applications. *Optical Materials* **62**, 152–158 (2016).
32. Wang, Z. *et al.* Giant photoluminescence enhancement in tungsten-diselenide-gold plasmonic hybrid structures. *Nature Communications* **7**, 11283 (2016).

33. Lee, K. C. J. *et al.* Plasmonic gold nanorods coverage influence on enhancement of the photoluminescence of two-dimensional mos2 monolayer. *Sci Rep.* **5**, 16374 (2015).
34. Sobhani, A. *et al.* Enhancing the photocurrent and photoluminescence of single crystal monolayer MoS₂ with resonant plasmonic nanoshells. *Appl. Phys. Lett.* **104**, 031112 (2014).
35. Gao, W. *et al.* Localized and continuous tuning of monolayer mos2 photoluminescence using a single shape-controlled ag nanoantenna. *Advanced Materials* **28**, 701–706 (2016).
36. Chen, H. *et al.* Manipulation of photoluminescence of two-dimensional mose2 by gold nanoantennas. *Sci Rep.* **6**, 22296 (2016).
37. Li, J. *et al.* Tuning the photo-response in monolayer mos2 by plasmonic nano-antenna. *Sci Rep.* **6**, 23626 (2016).
38. Galfsky, T. *et al.* Broadband enhancement of spontaneous emission in two-dimensional semiconductors using photonic hypercrystals. *Nano Lett.* **16**, 4940–4945 (2016).
39. Janisch, C. *et al.* Mos2 monolayers on nanocavities: enhancement in light-matter interaction. *2D Materials* **3**, 025017, http://stacks.iop.org/2053-1583/3/i=2/a=025017 (2016).
40. Zhu, Y. *et al.* Strongly enhanced photoluminescence in nanostructured monolayer mos2 by chemical vapor deposition. *Nanotechnology* **27**, 135706 (2016).
41. Noori, Y. J. *et al.* Photonic crystals for enhanced light extraction from 2d materials. *ACS Photonics* **3**, 2515–2520 (2016).
42. Lin, L.-L. & Li, Z.-Y. Interface states in photonic crystal heterostructures. *Phys. Rev. B* **63**, 033310 (2001).
43. Zhou, Y.-S., Gu, B.-Y. & Wang, F.-H. Guide modes in photonic crystal heterostructures composed of rotating non-circular air cylinders in two-dimensional lattices. *Journal of Physics: Condensed Matter* **15**, 4109–4118 (2003).
44. Palik, E. D. (ed.) *Handbook of Optical Constants of Solids* (Academic Press, Boston, 1985).
45. Klein, C. A. Room-temperature dispersion equations for cubic zinc sulfide. *Appl. Opt.* **25**, 1873–1875 (1986).
46. Yariv, A. & Yeh, P. (eds) *Optical Waves in Crystals: Propagation and Control of Laser Radiation* (Wiley-Interscience, New York, 1983).
47. Bendickson, J. M., Dowling, J. P. & Scalora, M. Analytic expressions for the electromagnetic mode density in finite, one-dimensional, photonic band-gap structures. *Phys. Rev. E* **53**, 4107 (1996).
48. Hofmann, S., Thomschke, M., Lüssem, B. & Leo, K. Top-emitting organic light-emitting diodes. *Opt. Express* **19**, A1250 (2011).
49. Deppe, D. G., Lei, C., Lin, C. C. & Huffaker, D. L. Spontaneous emission from planar microstructures. *Journal of Modern Optics* **41**, 325–344 (1994).
50. Yang, F.-F., Huang, Y.-L., Xiao, W.-B., Liu, J.-T. & Liu, N.-H. Control of absorption of monolayer mos2 thin-film transistor in one-dimensional defective photonic crystal. *Europhysics Letters* **112**, 37008 (2015).

Acknowledgements

Author Contributions
J. T. Liu supervised the project, did the theoretical derivation and the numerical calculation, analyzed the results, and wrote the paper. H. Tong, Z. H. Wu, and J. B. Wang analyzed of the results and wrote the paper. Y. S. Zhou supervised the project, analyzed the results, and wrote the paper. All authors discussed the results and commented on the manuscript.

Additional Information
Competing Interests: The authors declare that they have no competing interests.

Publisher's note: Springer Nature remains neutral with regard to jurisdictional claims in published maps and institutional affiliations.